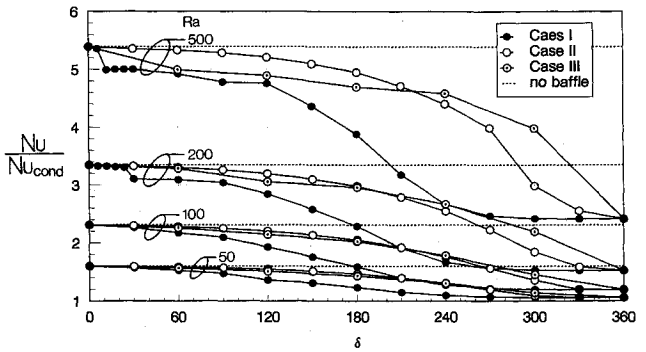

Fig. 2 Effects of baffle angular span on the heat transfer results.

It is easy to show that the conduction Nusselt number can be evaluated as

$$Nu_{cond} = \frac{1}{R_i \ln(R_0/R_i)} \tag{8}$$

The normalized Nusselt numbers are plotted in Fig. 2, from which it is confirmed that circumferential baffles are effective in reducing heat losses from a pipe insulation. The reduction in heat losses increases with the baffle angular span, and it reaches the maximum when the annulus is completely partitioned into two sections. For $Ra = 50$, the maximum reduction in heat loss is 34%, and it is 48, 54, and 55% for $Ra = 100$, 200, and 500, respectively.

Conclusions

In this study, the feasibility of using circumferential baffles to reduce convective heat losses from pipe insulation has been successfully demonstrated. It shows that the effectiveness of pipe insulation is directly proportional to its baffle angular extent. The maximum reduction in heat loss always occurs at $\delta = 360$ deg, when the pipe insulation is completely partitioned into two sections. This finding has an important implication for engineering practice: it is more effective to apply multiple layers of insulation, with each layer being separated by an impermeable partition, than to use only one single layer of insulation with the same thickness. This suggested practice is simple, but it is often overlooked by engineers.

References

[1]Bejan, A., and Anderson, R., "Heat Transfer Across a Vertical Impermeable Partition Imbedded in Porous Medium," *International Journal of Heat and Mass Transfer*, Vol. 24, No. 7, 1981, pp. 1237–1245.

[2]Bejan, A., "Natural Convection Heat Transfer in a Porous Layer with Internal Flow Obstructions," *International Journal of Heat and Mass Transfer*, Vol. 26, No. 6, 1983, pp. 815–822.

[3]Lai, F. C., "Improving Effectiveness of Pipe Insulation by Using Radial Baffles to Suppress Natural Convection," *International Journal of Heat and Mass Transfer*, Vol. 36, No. 4, 1993, pp. 899–906.

[4]Yang, H. Q., Yang, K. T., and Lloyd, J. R., "Natural Convection Suppression in Horizontal Annuli by Azimuthal Baffles," *International Journal of Heat and Mass Transfer*, Vol. 31, No. 10, 1988, pp. 2123–2135.

[5]Georgiadis, J. G., and Catton, I., "Dispersion in Cellular Thermal Convection in Porous Layers," *International Journal of Heat and Mass Transfer*, Vol. 31, No. 5, 1988, pp. 1081–1091.

[6]Nield, D. A., "The Limitation of the Brinkman-Forchheimer Equation in Modeling Flow in a Saturated Porous Medium and at an Interface," *International Journal of Heat and Fluid Flow*, Vol. 12, No. 3, 1991, pp. 269–272.

[7]Iyican, L., Bayazitoglu, Y., and Witte, L. C., "An Analytical Study of Natural Convective Heat Transfer Within a Trapezoidal Enclosure," *Journal of Heat Transfer*, Vol. 102, Nov. 1980, pp. 640–647.

Transient Compressible Flow in Variable Permeability Media

R. A. Polehn,* M. Keyhani,† and M. Parang‡
University of Tennessee, Knoxville, Tennessee 37996

Introduction

In many applications, decomposing polymers are subjected to rapid heating. The high temperatures induce chemical reactions within the polymer which cause the formation and flow of pyrolysis gases. Temperature gradients cause steep property variations, especially for permeability, which may vary by several orders of magnitude across the narrow pyrolysis zone. Accurate estimates of the pore pressure is required for mechanical stress and failure analysis of the polymer.

Pressure is predicted with the pore pressure equation, which is a combination of the conservation of mass and Darcy's law for porous media. For transient one-dimensional compressible flow, the pore pressure equation is

$$\frac{\partial}{\partial x}\left(\rho \frac{K}{\mu}\frac{\partial P}{\partial x}\right) = \frac{\partial}{\partial t}(\phi\rho) \tag{1}$$

where P is pressure, ρ is fluid density, μ is fluid viscosity, K is permeability, and ϕ is porosity. For highly compressible flow, both Muskat[1] and Morrison[2] have presented exact solutions to the pore pressure equation. Neither successful measurement of pore pressure in a decomposing composite, nor exact transient solutions to Eq. (1) for variable permeability compressible flow, were found in the literature.

Model

An isothermal variable permeability exact solution, suitable for verification purposes, will be developed for the pore pressure equation. The schematic of the problem, and boundary and initial conditions, are shown in Fig. 1a. In the pyrolysis zone the permeability varies approximately exponentially with distance. However, the exponential function is not very suitable for an exact solution; thus another, somewhat more severe assumption, is that the permeability varies nearly inversely with distance. For a given permeability change, Fig. 1b compares the exponential function to the assumed permeability variation, shown as follows:

$$K = \frac{K_L}{x/L + K_L/K_s} \qquad 0 < K_L/K_s << 1 \tag{2}$$

where L is the distance from the surface to the point where $K = K_L$, which is considered the edge of the domain for computational purposes. Equation (2) and the ideal gas law can be substituted into Eq. (1) to obtain

$$\frac{\partial}{\partial x}\left(\frac{K_L}{x/L + K_L/K_s}\frac{PM}{\mu RT}\frac{\partial P}{\partial x}\right) = \frac{\partial}{\partial t}\left(\phi\frac{PM}{RT}\right) \tag{3}$$

For this study, the porosity, viscosity, temperature T, and molecular weight M, are assumed constant. For a step bound-

Received March 25, 1993; revision received Sept. 20, 1993; accepted for publication Sept. 20, 1993.

*Graduate Student, Mechanical and Aerospace Engineering Department.

†Associate Professor, Mechanical and Aerospace Engineering Department.

‡Professor, Mechanical and Aerospace Engineering Department.

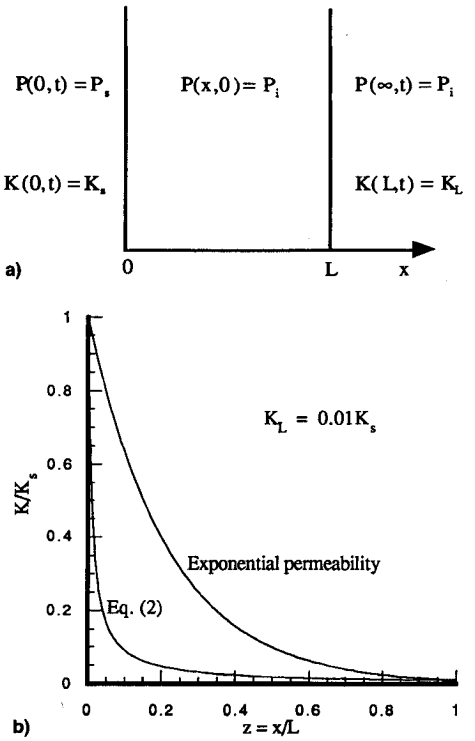

Fig. 1 Problem statement: a) geometry and boundary conditions and b) comparison of exponentially varying permeability with the assumed variation.

ary condition at the surface, Eq. (3) is normalized as

$$\frac{\partial}{\partial z}\left[\frac{\nu + Q}{z + \varepsilon}\frac{\partial Q}{\partial z}\right] = \frac{\partial Q}{\partial \tau}$$

$$Q(0, t) = 1 \qquad Q(\infty, t) = 0 \qquad Q(z, 0) = 0 \tag{4}$$

where

$$z = \frac{x}{L} \quad Q = \frac{P - P_i}{P_s - P_i} \quad \nu = \frac{P_i}{P_s - P_i} \quad \tau = \frac{K_L(P_s - P_i)t}{\mu\phi L^2}$$

where P_s is the surface pressure, P_i is the initial pressure, and the small parameter is $\varepsilon = K_L/K_s$. A regular perturbation expansion scheme for normalized pressure in terms of the small parameter (ε)

$$Q = Q_0 + \varepsilon Q_1 + \mathcal{O}(\varepsilon^2) \tag{5}$$

can be introduced into Eq. (4) to generate a set of equations valid for various orders of magnitude of the small parameter (ε). Thus, for $z = \mathcal{O}(1)$, we have to the first-order

$$-(\nu + Q_0)\frac{\partial Q_0}{\partial z} + z\frac{\partial}{\partial z}\left[(\nu + Q_0)\frac{\partial Q_0}{\partial z}\right] = z^2\frac{\partial Q_0}{\partial \tau}$$

$$Q_0(0, t) = 1 \qquad Q_0(\infty, t) = 0 \qquad Q_0(z, 0) = 0 \tag{6}$$

Similarly, the $\mathcal{O}(\varepsilon)$ equation and boundary conditions are

$$-(\nu + Q_0)\frac{\partial Q_1}{\partial z} - Q_1\frac{\partial Q_0}{\partial z} + \frac{\partial}{\partial z}\left[(\nu + Q_0)\frac{\partial Q_0}{\partial z}\right] + z\frac{\partial}{\partial z}\left[(\nu + Q_0)\frac{\partial Q_1}{\partial z}\right] + z\frac{\partial}{\partial z}\left[Q_1\frac{\partial Q_0}{\partial z}\right] = 2z\frac{\partial Q_0}{\partial \tau} + z^2\frac{\partial Q_1}{\partial \tau}$$

$$Q_1(0, t) = 0 \qquad Q_1(\infty, t) = 0 \qquad Q_1(z, 0) = 0 \tag{7}$$

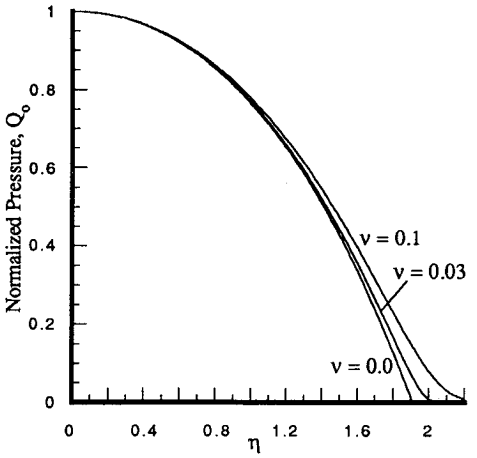

Fig. 2 Order (1) pressure profiles.

Order (1) Solution

Equation (6) can be cast as an ordinary differential equation using the similarity relation

$$Q_0 = y_0(z/\tau^{1/3}) = y_0(\eta) \tag{8}$$

to obtain

$$(\nu + y_0)\ddot{y}_0 + \dot{y}_0\dot{y}_0 - \frac{(\nu + y_0)\dot{y}_0}{\eta} + \frac{\dot{y}_0\eta^2}{3} = 0$$

$$y_0(0) = 1 \qquad y_0(\infty) = 0 \tag{9}$$

For the case of an initial vacuum, at the wave front both ν and y_0 are zero. Thus, at the wave front, Eq. (9) simplifies to two terms and a relationship between the wave front location η_F and the slope of the pressure profile is obtained

$$\dot{y}_0[\dot{y}_0 + (\eta_F^2/3)] = 0 \tag{10}$$

Using Eq. (10) to obtain the initial slope, Eq. (9) was integrated numerically from the wave front by the shooting method, using a fourth-order Runge-Kutta method, to match the boundary condition $y_0(0) = 1$. The $\mathcal{O}(1)$ solution is shown in Fig. 2. The shape of the profile is approximately parabolic, which is a characteristic shape often seen for the nonlinear pore pressure equation. Note that for $\varepsilon = 0$, the permeability becomes infinitely large at the surface and, consistent with this, the slope of the pressure solution drops to zero at $\eta = 0$. The normalized mass stored per unit flow area is defined as

$$M_N = \frac{\int_0^{z_F}(\rho - \rho_i)\,dz}{\int_0^1(\rho_s - \rho_i)\,dz} \tag{11}$$

where $z_F < 1.0$. For this isothermal problem, the density difference, $\rho - \rho_i$, can be related through the ideal gas law to the pressure difference, $P - P_i$, and from there to the normalized pressure. For the $\mathcal{O}(1)$ solution, Eq. (8) gives the remaining relationship required to normalize Eq. (11) and obtains

$$M_N = \tau^{1/3}\int_0^{\eta_F} y_0\,d\eta \tag{12}$$

Equation (12) was integrated numerically. Let the normalized speed be defined as

$$U = \frac{K_L(P_s - P_i)u}{\mu\phi L} \tag{13}$$

Table 1 Order (1) solution[a] characteristics

Variable	$\nu = 0.00$	$\nu = 0.03$[b]	$\nu = 0.10$[b]
z_F	$1.91116\tau^{1/3}$	$1.99654\tau^{1/3}$	$2.18417\tau^{1/3}$
U_F	$0.63705\tau^{-2/3}$	$0.66551\tau^{-2/3}$	$0.72806\tau^{-2/3}$
M_N	$1.31986\tau^{1/3}$	$1.34149\tau^{1/3}$	$1.38888\tau^{1/3}$

[a]Solution good until wave front reaches $z = 1.0$.
[b]Wave front is where pressure has risen 1%, $Q = 0.01$.

Then the wave front speed is

$$U_F = \tfrac{1}{3}\eta_F\tau^{-2/3} \tag{14}$$

Table 1 lists the wave front location and speed, and mass stored for several values of ν. Note that at time $\tau = 1.0$, the initial vacuum wave front has bypassed the characteristic length for the problem. Because this wave front reaches $z = 1.0$ just after $\tau = 0.1$, the similarity solution is good only for early times, up to approximately $\tau = 0.1$.

The $\mathcal{O}(1)$ and finite initial pressure ($\nu > 0.0$) solution is also shown in Fig. 2. This problem was also solved using the shooting method beginning near the wave front. The results show that the presence of a finite initial pressure causes diffusion at the wave front and results in faster movement of the gas into the porous material. Morrison,[2] in his constant permeability solution, showed that a finite initial pressure transforms the solution of the pore pressure equation from a purely wavelike to a more diffusive solution near the wave front. These results agree and confirm the same trend as those of Morrison. As an interesting note, Pascal[3] showed that the flow of non-Newtonian power law fluids in porous media also displays wavelike characteristics.

Order (ε) Correction

The permeability, although comparatively high, is not infinite at the surface. Thus, Eq. (7) must be solved to obtain more realistic pressure profiles. The $\mathcal{O}(\varepsilon)$ correction can be expressed using the similarity variables

$$Q_1 = \tau^{-1/3}y_1(z/\tau^{1/3}) = \tau^{-1/3}y_1(\eta) \tag{15}$$

Substituting these variables into Eq. (7), the following ordinary differential equation, with boundary conditions, is obtained:

$$(\nu + y_0)\ddot{y}_1 + \left[-\frac{(\nu + y_0)}{\eta} + 2\dot{y}_0 + \frac{\eta^2}{3}\right]\dot{y}_1 + \left[-\frac{\dot{y}_0}{\eta} + \ddot{y}_0 + \frac{\eta}{3}\right]y_1 + \left[\frac{\dot{y}_0\dot{y}_0}{\eta} + \frac{(\nu + y_0)\ddot{y}_0}{\eta} + \frac{2\dot{y}_0\eta}{3}\right] = 0$$

$$y_1(0) = 0 \qquad y_1(\infty) = 0 \tag{16}$$

Equation (16) was also numerically solved via the Runge-Kutta method. The $\mathcal{O}(\varepsilon)$ and initial vacuum similarity correction is shown in Fig. 3. Unlike the $\mathcal{O}(1)$ solution, the correction slope (-0.42703 at $\eta = 0$) does not drop to zero at the surface. This is true because permeability does not become infinite at the surface, and therefore, a finite pressure difference (slope) is required to move the fluid. The finite initial pressure similarity correction demonstrates that the initial vacuum correction must drop back to zero just beyond the wave front.

The correction itself, Q_1, is a function of time in two ways, once through the similarity variable, and in addition through the coefficient $\tau^{-1/3}$ in Eq. (15). The correction becomes smaller as time goes on, i.e., the pressure profile approaches that for the $\mathcal{O}(1)$ solution. Thus, the fact that there is a finite permeability at the surface becomes less important as time progresses. Figure 4 shows the normalized pressure variations for a relatively large ε. Not shown, but as expected as ε becomes smaller, the time variant curves become closer together near the limiting case defined by the $\mathcal{O}(1)$ solution.

Comparison to Finite Difference Computation

The finite difference method used is based on the concept of the control volume and control volume face as defined by Pantankar.[4] For the algebraic approximation to Eq. (4), Polehn[5] evaluated the relative merits of various schemes for computation of the effective diffusion coefficient and recommended properties be evaluated at the control volume face. If a required flow property is not known directly, the property is evaluated based on the nominal (interpolated) temperatures/pressures at the control volume face. Thus, for the normalized Eq. (4), the effective diffusion coefficient is

$$\Psi_{\text{EFF}} = \left(\frac{Q + \nu}{z + \varepsilon}\right)_{\text{FACE}} \tag{17}$$

and the one-dimensional finite difference approximation to Eq. (4) is

$$\left(\Psi_{\text{EFF}}\frac{\Delta Q}{\Delta z}\right)_e - \left(\Psi_{\text{EFF}}\frac{\Delta Q}{\Delta z}\right)_w = \frac{Q - Q^0}{\Delta\tau} \tag{18}$$

The finite difference equations were solved implicitly and iterated to convergence for a uniform mesh of 51 nodes and

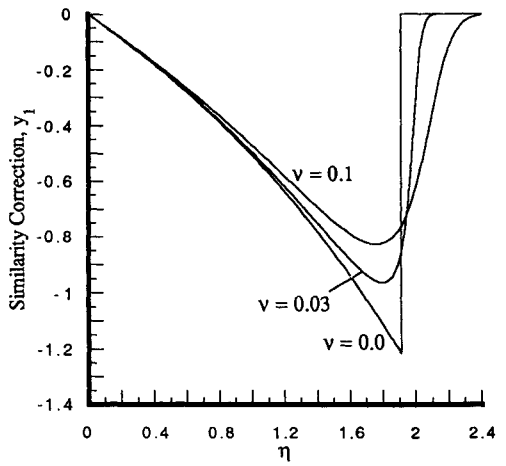

Fig. 3 Order (ε) similarity correction for pressure profiles.

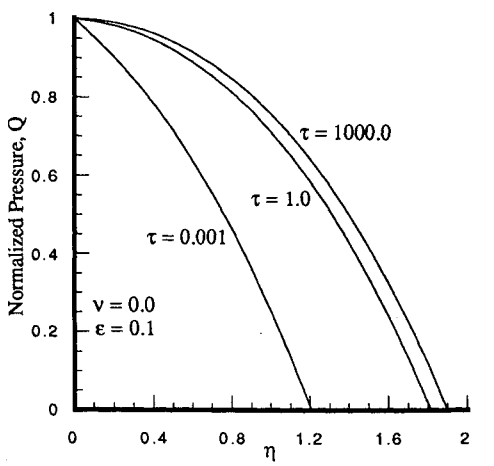

Fig. 4 Order (ε) perturbation solution for pressure ($\nu = 0.0$, $\varepsilon = 0.1$).

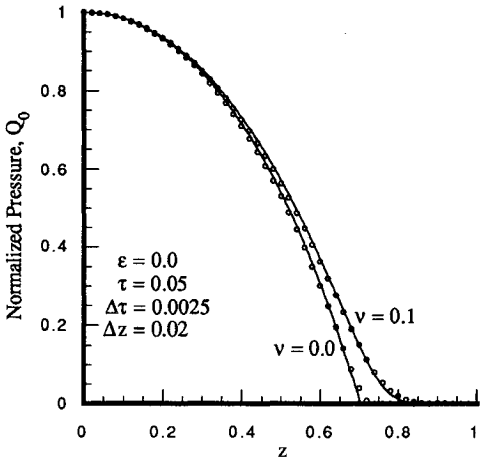

Fig. 5 Comparison of finite difference prediction to exact $\mathcal{O}(1)$ solution at $\tau = 0.05$.

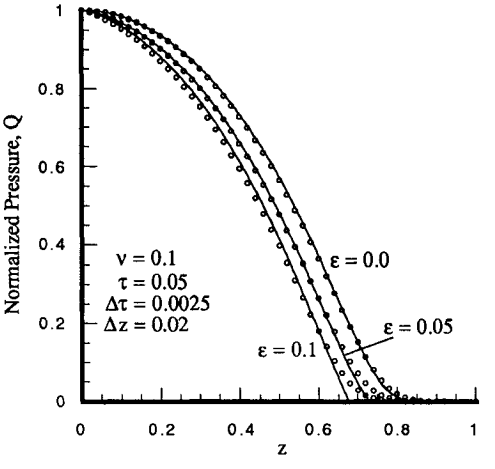

Fig. 6 Comparison of finite difference prediction to the perturbation solution for various values of small parameter ε at $\tau = 0.05$ and $\nu = 0.1$.

20 uniform time steps. An early time of $\tau = 0.05$ was chosen to confine the solution to the region $0 \leq z \leq 1.0$.

Figure 5 compares the exact $\mathcal{O}(1)$ solution to the finite difference prediction. For this figure, the deviation between the computational points and the exact solution is solely due to the finite difference approximation. Note that for the case of an initial vacuum ($\nu = 0$), the largest discrepancy occurs at the wave front. Because the finite difference equations are diffusive in nature, the case of a finite initial pressure ($\nu = 0.1$) is handled at the wave front more accurately than the wavelike initial vacuum case.

On the other hand, the $\mathcal{O}(\varepsilon)$ perturbation solution is generally satisfactory except at the wave front. As ε becomes large, the additive nature of the perturbation approximation removes the diffusive tail and causes the $\mathcal{O}(\varepsilon)$ solution to incorrectly assume a sharp wave front. Figure 6 shows that the finite difference approximation follows the $\mathcal{O}(\varepsilon)$ solution well until the wave front is reached. Additional refinement of the finite difference mesh and time step changes the finite difference solution somewhat, but does not come close to matching the ($\varepsilon = 0.1$) perturbation solution at the wave front.

Conclusions

A similarity solution is presented for transient compressible isothermal flow through porous media in which the permeability varies inversely with distance. A modification of the exact $\mathcal{O}(1)$ solution was derived by a regular perturbation method for the case of a finite permeability at the surface.

The finite difference approximation was used to identify a weakness in the perturbation correction at the wave front when both the initial pressure and the small parameter (ε) become large and significant. In all other aspects, the finite difference prediction agreed quite well with the perturbation solution.

Acknowledgment

Financial support of this work under NASA Grant NAG8-862 is gratefully acknowledged.

References

[1]Muskat, M., "The Flow of Compressible Fluids Through Porous Media and Some Problems in Heat Conduction," *Physics*, Vol. 5, March, 1934, pp. 71–94.

[2]Morrison, F. A., "Transient Gas Flow in a Porous Column," *Industrial Engineering Chemistry Fundamentals*, Vol. 11, No. 2, 1972, pp. 191–197.

[3]Pascal, H., "On Non-Linear Effects in Unsteady Flows Through Porous Media," *International Journal of Non-Linear Mechanics*, Vol. 26, No. 2, 1991, pp. 251–261.

[4]Pantankar, S. V., *Numerical Heat Transfer and Fluid Flow*, 1st ed., Hemisphere, New York, 1980, Chap. 3.

[5]Polehn, R. A., "Thermal Response of an Axisymmetric, Charring-Decomposing Polymer," Ph.D. Dissertation, Univ. of Tennessee at Knoxville, Knoxville, TN, in progress.

Effects of Nonequilibrium Chemistry on the Reference Temperature Method and Reynolds Analogy

James D. Ott* and John D. Anderson Jr.†
University of Maryland,
College Park, Maryland 20742

Nomenclature

M_e = Mach number at the edge
T = temperature, K

Subscripts
e = edge condition
F = quantity evaluated using correlation factor
w = wall condition

I. Introduction

IN the development of hypersonic vehicles, the accurate prediction of heat transfer and skin friction is required. One way to predict these values is by using a reference temperature method to find the skin friction, and then to use Reynold's analogy to calculate the heat transfer through the Stanton number. These methods were developed for nonreacting air and may not be accurate for nonequilibrium chemically reacting air. The purpose of this study is to determine what effect nonequilibrium air chemistry has on the reference temperature method and Reynold's analogy; then to correlate a modification to the reference temperature method to make

Received June 1, 1993; revision received Sept. 14, 1993; accepted for publication Sept. 30, 1993.

*Graduate Assistant, Hypersonic Group, Department of Aerospace Engineering. Student Member AIAA.

†Professor, Department of Aerospace Engineering. Fellow AIAA.